Analysis of Tau Polarimetry PID Selectors Systematics and Testing of the Belle II Analysis Software

IPP Summer Student Fellowship Report

Gillian Godden

Supervisors: Michael Roney and Caleb Miller

September 7, 2020

Contents

1   Introduction

The Belle II experiment is a successor to the Belle experiment located at the SuperKEKB accelerator complex at KEK. Using the SuperKEKB e^+e^- collider and the planned upgrades to it, Belle II plans to use an electron beam with a polarization of approximately 70% to probe for new physics through precision electroweak measurements such as the weak neutral current vector coupling constants of the b-quarks, c-quarks and muons [1].

To make these precision measurements, the average polarization of the electron beam must be known with an uncertainty less than $\pm 0.5\%$. One method of measuring the polarization is through e^+e^- transitions to tau pairs, specifically to $\tau + \tau^- \to \pi^+ \bar{\nu}_\tau + \rho^- \nu_\tau$ decays. These were chosen over other tau decays due to their high polarization sensitivity in the $\tau \to \pi \nu_\tau$ decay, high statistics, and relative purity. As taus decay within the detector, the kinematics of the final state particles can be used to get information on the tau spin and the average polarization of the electron beam through polarization fits.

This method of measuring the average polarization of the electron beam through polarization fits had already been developed by Caleb Miller. This report covers the investigations into the effect PID selectors have on polarization fits, the determination of systematic errors associated with the PID selectors, and attempts to improve agreement between monte carlo data and detector data all while using BaBar data. This report also covers the testing of the Belle II analysis software for the purpose of implementing the tau polarimetry technique using Belle II monte carlo.

2   Analysis Methods

Using the BaBar analysis tools, non-polarized monte carlo (which included tau, bhabha, muon, uds, and $c\bar{c}$ monte carlo) and detector data were processed through the BaBar analysis software to reconstruct events where e^+e^- transitions to the tau pair with decays $\tau \to \pi \nu_\tau$ (known as the signal track) and $\tau \to \rho \nu_\tau$ (known as the tag track). These reconstructed $\tau + \tau^- \to \pi^+ \bar{\nu}_\tau + \rho^- \nu_\tau$ decay events were stored in root files for additional analysis as done in this report. A similar process was

done using the Belle II analysis tools and Belle II monte carlo.

When analyzing this monte carlo and detector data, there were a few tools used repeatedly. These analysis methods are explained below.

2.1 Polarization Fits

Polarization fits are designed to give the average polarization of the inputted data. This is done using a Barlow template fit. Barlow template fits are done by taking templates of different components that make up the data and varying the contribution of those templates to determine the combination that provides the best fit that models the data [2]. In the case of these polarization fits, the distribution being fit is a 2D histogram of the centre of mass momentum and centre of mass $\cos\theta$ of the signal track pion. Templates are made using fully left and right polarized monte carlo. Contributions from these templates are varied until the combination of left and right polarized beams that best fit the data is determined. As the data was unpolarized, a 50/50 contribution from the left and right polarized beam templates, resulting in a net polarization of zero, was expected.

It should be noted that fits are initially done on the positively charged tracks and the negatively charged tracks separately as the tracks themselves have opposite polarization sensitivity. The combined average of the two fits gives the average polarization of the beams. Thus the format of the output of the polarization fit is as seen in Table 1 where P_i^+ is the polarization fit for the positively charged track, P_i^- is the fit for the negatively charged track, P_i^A is the combined averaged of the positive and negative charged fits, and $\sigma_i^{+,-,A}$ is the error in the positively charged fit, negatively charged fit, and the combined average respectively. Within the table, sample 1-3 corresponds to monte carlo data while data corresponds to detector data. Polarization fits are done on monte carlo data in addition to detector data to confirm that the fits are working as expected and that no biases are introduced during analysis. As the monte carlo data contains a larger number of events than the detector data does, the monte carlo data is split up into 3 samples of similar size to the detector data.

Though the polarization fits themselves can be used to determine whether the fits are reasonable, if one polarization fit is compared to another and both fits look

3

	Positive Charge	Negative Charge	Combined Average
Sample 1	$P_1^+ \pm \sigma_1^+$	$P_1^- \pm \sigma_1^-$	$P_1^A \pm \sigma_1^A$
Sample 2	$P_2^+ \pm \sigma_2^+$	$P_2^- \pm \sigma_2^-$	$P_2^A \pm \sigma_2^A$
Sample 3	$P_3^+ \pm \sigma_3^+$	$P_3^- \pm \sigma_3^-$	$P_3^A \pm \sigma_3^A$
Data	$P_D^+ \pm \sigma_D^+$	$P_D^- \pm \sigma_D^-$	$P_D^A \pm \sigma_D^A$

Table 1: Format of the outputted polarization fit.

reasonable, it is difficult to use the fits on their own to determine which fit is better. As such, a goodness of fit score was created to judge how good a fit was when compared to another fit. The formula for this score can be seen in Equation 1.

$$S_i = (P_i^A - 0)^2 + (\sigma_i^A)^2 + (P_i^+ - P_i^-)^2 \tag{1}$$

The goodness of fit score consists of three uncertainties. The first is a bias associated with a shift between the combined average value and the expected average polarization (0 for unpolarized beams), the second is the statistical uncertainty in the combined average, and the final one is a bias in the difference between the positive and negative polarization fits. The idea is the smaller these uncertainties are, the better the fit is. In addition to that, it is also expected that the statistical uncertainty would be larger than the other two uncertainties for a "good" fit. As such, this can also be used as a measure of how good the polarization fit is.

2.2   Monte Carlo and Data Histograms

Plotting is another useful method of analysis used in this report. As previously stated, monte carlo as well as detector data went through a reconstruction process resulting in root files containing only monte carlo and detector data that successfully passed the reconstruction requirements. Using this monte carlo and detector data, histograms of different variables can be created. Note that a luminosity scaling is applied to all monte carlo histograms created as the number of monte carlo events generated for a given particle is not an accurate reflection of the total number of those particles that would be detected in the detector. Luminosity scaling is described more in Section 3.3.

4

With the luminosity scaling, the monte carlo is coloured according to its type, with the tau monte carlo being further split and coloured according to decay mode. The coloured monte carlo is then stacked and plotted simultaneously with the data points for comparison. These histograms were produced for each variable used in the analysis, Figure 1 is an example showing the pion centre of mass $\cos\theta$ (ctcm) distribution for the negatively charged signal tracks.
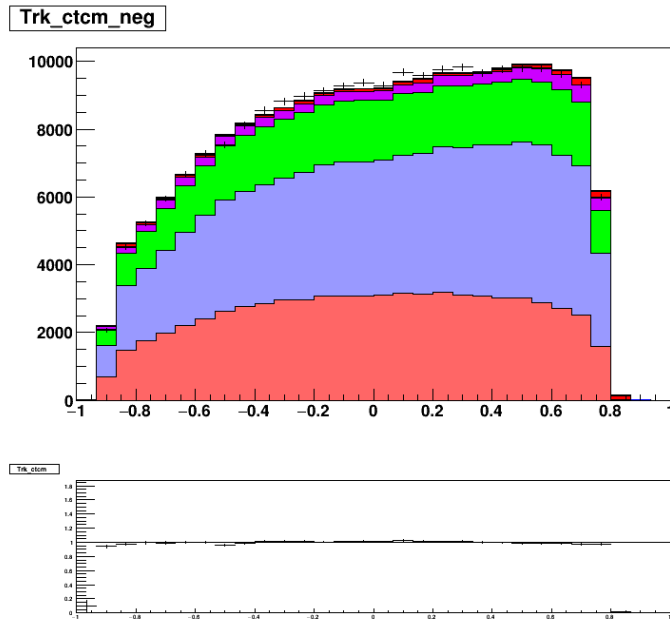
Figure 1: $\cos\theta$ distribution for negatively charged signal track (top). See Table 2 for colour scheme. Ratio of detector data and monte carlo (bottom).

Figure 1 shows a comparison between detector data and monte carlo data for for negatively charged signal track ctcm, where the points are the detector data and the colours are the various types of monte carlo listed in Table 2.

There are non-tau decay muons as well as uds and c$\bar{\text{c}}$ monte carlo, but they did not make up a significant portion of the monte carlo data and are therefore not visible. $\tau \to \rho\nu_\tau$ monte carlo is not seen in Figure 1 but will be seen in histograms in Section 4. Figure 1 also shows in the bottom plot the ratio between monte carlo and detector data, called the ratio histogram for the rest of this report, which is useful for determining the agreement between monte carlo and detector data.

5

Monte Carlo	Colours
$\tau \to e\nu_\tau \bar{\nu}_e$	Light red
$\tau \to \mu\nu_\tau \bar{\nu}_\mu$	Light blue
$\tau \to \pi\nu_\tau$	Green
$\tau \to \rho\nu_\tau$	Orange
$\tau \to$ else	Purple
Bhabhas	Red
Muons	Blue
uds	Yellow
$c\bar{c}$	Pink

Table 2: Monte carlo colour scheme.

During the analysis seen in Sections 3.2 and 3.3, it should be noted that while histograms of other variables were created, for the sake of brevity, only histograms of negatively changed signal track ctcm will be shown in this report.

2.3 χ^2 and Agreement

In Section 3.3, a method for measuring agreement was needed. One way the agreement between monte carlo and detector data can be measured is by calculating $\frac{\chi^2}{N}$ where χ^2 is given by Equation 2. R is the bin content of the ratio histogram, σ^R is the error in that bin content, and N is the total number of bins in the ratio histogram. $\frac{\chi^2}{N}$ closer to 1 indicates better agreement while $\frac{\chi^2}{N}$ farther away from 1 indicates worse agreement.

$$\chi^2 = \sum_{i=1}^{N} \left(\frac{R-1}{\sigma^R} \right)^2 \tag{2}$$

When this calculation was done during analysis, it was done for all the ratio histograms of the different variables. As only histograms of the negatively charged signal track ctcm are shown in this report, only $\frac{\chi^2}{N}$ for those histograms are listed in this report. Note that during the analysis seen in Section 3.3, $\frac{\chi^2}{N}$ was calculated for histograms of other variables as part of that analysis.

3 The BaBar Experiment

3.1 Introduction

The BaBar experiment was a detector at the e^+e^- collider, PEP-II, located at the SLAC National Accelerator Laboratory. While the polarimetry measurement technique will be used for measurements in the Belle II experiment, BaBar data was used for developing and optimizing the polarization fits. The reason for this is that, while Belle II had collected some data, at the time of writing this report the amount of data collected was minimal compared to the BaBar experiment. Belle II's analysis tools were also not as refined as BaBar's. As such, it was determined that it was best to start with BaBar data instead of Belle II data to develop the polarization measurement technique and identify dominant systematics.

With the BaBar data, analysis was done to determine PID selectors that improved polarization fits, methods were developed to estimate the error in those PID selectors, and an investigation was done into the cause of the disagreement between monte carlo data and detector data. This section covers the results of these studies.

3.2 Particle Identification (PID) Studies

When conducting polarization fits and creating histograms using both monte carlo and detector data, requirements for those fits and histograms included that

- events were selected by the BaBar Tau background filter (BGF)
- there were two charged tracks
- the sum of all charged tracks was zero
- there were zero neutrals in the signal track's hemisphere
- A π^0 in the tag hemisphere had
  - mass between 0.115 GeV and 0.15 GeV if there were two neutrals
  - likelihood greater than 45 if there was 1 neutral

- transverse event momentum (P_T) was greater than 1.2 GeV

Despite these requirements, monte carlo data still contained many bhabhas, $\tau \rightarrow e\nu_\tau \bar{\nu}_e$ decays, $\tau \rightarrow \mu\nu_\tau \bar{\nu}_\mu$ decays, and other tau decays. With the hopes of eliminating more electrons and muons from the data, another requirement was added that required the signal track to fail a given electron and muon PID selector. As it was unknown which electron and muon selectors should be used, further investigation was done into the selectors to determine which selectors provided the best fit. The electron and muon PID selector options investigated are shown in Table 3.

Electron Selector (E)	Name
1	VeryLooseElectronMicroSelection
2	LooseElectronMicroSelection
7	VeryLooseKMElectronMicro
8	LooseKMElectronMicro
Muon Selector (M)	Name
1	VeryLooseMuonMicroSelection
2	LooseMuonMicroSelection
5	NNVeryLooseMuonSelection
6	NNLooseMuonSelection
16	BDTVeryLooseMuonSelection
17	BDTLooseMuonSelection
20	BDTVeryLooseMuonSelectionFakeRate
21	BDTLooseMuonSelectonFakeRate

Table 3: Electron and muon selectors' names and corresponding numbers.

These selectors were tested over the other selectors because they were the loose or very loose versions of the selectors. As such, they were expected to select more particles than the tight versions of the selectors, which was the desired result. To determine which electron and muon PID selectors should be investigated further, histograms using the previously listed cuts and electron and muon selector combinations were created as seen in the examples in Figure 2. See Appendix A for other histograms created. These histograms were then compared to the other histograms with different selector combinations to determine which selectors cut out the most electrons and muons while cutting out the fewest pions. Through this

comparison, it was determined that further investigation should be done into electron selectors = 1, 7, 8, which appeared to cut out the most electrons, and muon selectors = 16, 20, 21, which appeared to cut out the most muons.
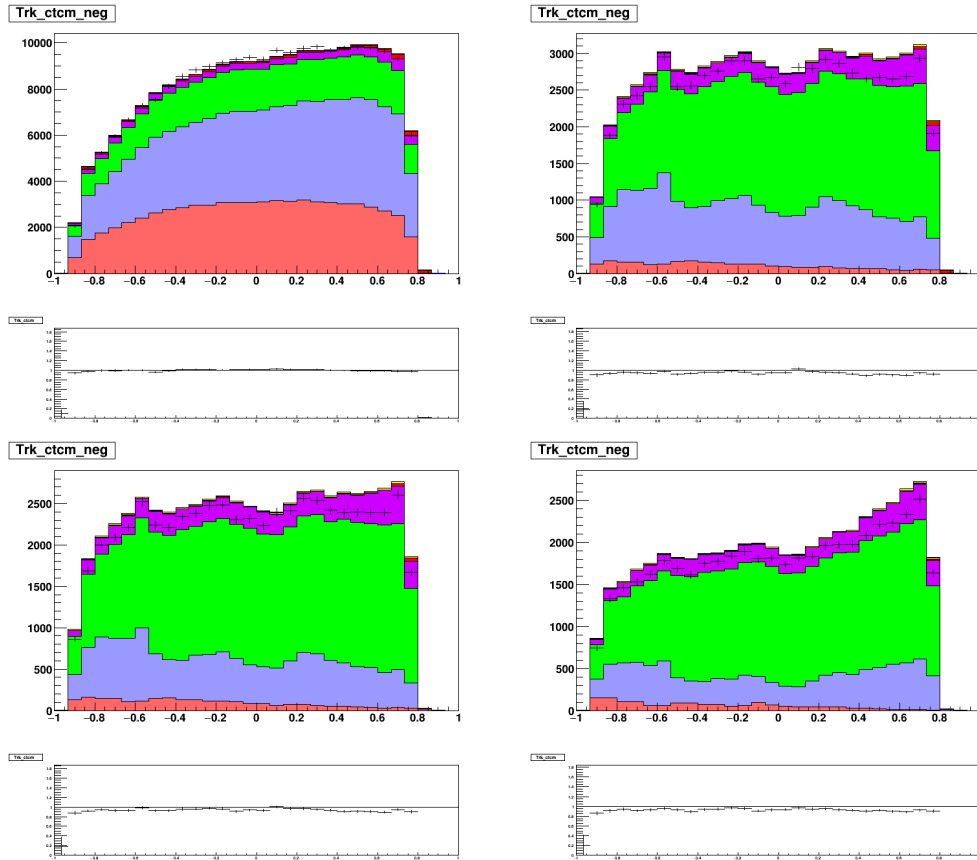
Figure 2: Histogram with no PID selectors (top left), Histogram with electron selector = 8, muon selector = 21 (top right), Histogram with electron selector = 7, muon selector = 20 (bottom left), Histogram with electron selector = 1, muon selector = 16 (bottom right). See Table 2 for colour scheme.

Polarization fits were then done on the detector data for each electron and muon PID selector pair from the narrowed down list. Using Equation 1, goodness of fit scores were calculated from the polarization fits, the results of which can be seen in Table 4. Based on the fact that electron selector = 1 and muon selector = 20 both had the smallest goodness of fit score and that $\sigma_i^{A^2}$ was the largest component of

the goodness of fit score, these results suggested that those selectors were the best selectors to use in the polarization fits.

PID Selectors	$(P_i^A - 0)^2$	$(\sigma_i^A)^2$	$(P_i^+ - P_i^-)^2$	Total Score
E = 8, M = 21	0.00001296	0.00046225	0.00403225	0.00450746
E = 8, M = 20	0.00001521	0.00041209	0.00187489	0.00230219
E = 8, M = 16	0.00018225	0.00041209	0.00252004	0.00311438
E = 7, M = 21	0.00005625	0.00045369	0.00763876	0.00814870
E = 7, M = 20	0.00000009	0.00040401	0.00423801	0.00464211
E = 7, M = 16	0.00033489	0.00040401	0.00527076	0.00600966
E = 1, M = 21	0.00006400	0.00051529	0.00169744	0.00227673
E = 1, M = 20	0.00000400	0.00045369	0.00035721	0.00081490
E = 1, M = 16	0.00020449	0.00045796	0.00033124	0.00099369

Table 4: Goodness of fit scores for the polarization fits when using different PID selector combinations.

As previously stated, the average polarization of the beams must be known with an uncertainty of less than $\pm 0.5\%$. While the polarization fits do output the statistical uncertainty of the fits, there were still systematic uncertainties, including ones associated with the PID selectors, that needed to be considered. Thus to determine the total uncertainty of the polarization fits, the systematic uncertainty associated with the PID selectors needed to be estimated.

One method of estimating the systematic uncertainty was through investigating the effect of PID tweaking; PID tweaking refers to a tweaking of the acceptance of the PID algorithms so that PID selection performs similarly on both monte carlo data and detector data. This was done by taking detector data where there was PID tweaking and data where there was no PID tweaking, applying the same cuts and selectors to both data, performing polarization fits and calculating the goodness of fit scores for both data, then calculating the difference between goodness of fits scores when there was PID tweaking versus when there wasn't PID tweaking. The results of this can be seen in Table 5. From this, we see that electron selector = 1 and muon selector = 16 had the smallest difference between goodness of fit scores of 0.00742498. If this is taken to be the systematic variance, then the systematic uncertainty would be approximately 8.62%. As the polarization fits needed to have an overall max uncertainty of $\pm 0.5\%$, this was to large to use.

Another method of estimating the systematic uncertainty of the PID selectors was

PID Selectors	$(P_i^A - 0)^2$ Diff	$(\sigma_i^A)^2$ Diff	$(P_i^+ - P_i^-)^2$ Diff	Total Score Diff
E = 8, M 21	0.00001175	-0.00006216	-0.02315976	-0.02321017
E = 8, M 20	-0.00001183	-0.00003735	-0.01305795	-0.01310713
E = 8, M 16	0.00013736	-0.00003312	-0.00813020	-0.00802596
E = 7, M 21	0.00002376	-0.00005707	-0.03003605	-0.03006936
E = 7, M 20	-0.00000247	-0.00003699	-0.01790343	-0.01794289
E = 7, M 16	0.00016065	-0.00003280	-0.01168128	-0.01155343
E = 1, M 21	-0.00008976	0.00000000	-0.03245360	-0.03254336
E = 1, M 20	-0.00011700	-0.00002592	-0.01688248	-0.01702540
E = 1, M 16	0.00020424	-0.00002165	-0.00760757	-0.00742498

Table 5: Difference in goodness of fit scores when there was PID tweaking versus when there wasn't PID tweaking using the different PID selector combinations.

through investigating the difference between PID selectors. First polarization fits were done on both monte carlo data and detector data using the different selector combinations. Then the shifts in the polarization fit of the monte carlo samples when selectors were changed from a base set of selectors, electron selector = 1 and muon selector = 16, to another combination of selectors was calculated. The same shift was also calculated with the detector data. Then the differences between the detector data shift and each of the monte carlo sample shifts were calculated. Finally, the average and standard deviation of those differences was calculated. An example of this can be seen in Table 6. The goal was to measure the relative difference between the shift in the monte carlo combined average and the shift in the detector data combined average when selectors were changed.

A table of these averages with the different PID selector combinations is shown in Table 7. It should be noted at this point a requirement that $\cos\theta$ be between -0.8 and 0.8 was added due to a disagreement between monte carlo and detector data in the bhabhas. This disagreement was later fixed after applying boost and momentum corrections but at the time of this analysis, these corrections had not yet been applied.

Taking the average standard deviation of the rows and columns, the systematic uncertainty in the muon selector was found to be $\sigma_\mu = 0.00328$ and the systematic uncertainty in the electron selector was found to be $\sigma_e = 0.00021$. Varying the columns and rows individually by their statistical uncertainty and re-calculating

E = 1, M = 16	Positive Charge	Negative Charge	Combined Average
Sample 1	-0.0372	-0.0142	-0.0252
Sample 2	-0.0546	-0.0222	-0.0377
Sample 3	0.0029	-0.0239	-0.0110
Data	0.0212	-0.0118	0.0040
E= 7, M= 16	Positive Charge	Negative Charge	Combined Average
Sample 1	-0.0369	-0.0148	-0.0254
Sample 2	-0.0542	-0.0226	-0.0378
Sample 3	0.0024	-0.0242	-0.0114
Data	0.0227	-0.0131	0.0040
Shifts	Positive Charge	Negative Charge	Combined Average
Sample 1 Shift	-0.0003	0.0006	0.0002
Sample 2 Shift	-0.0004	0.0004	0.0001
Sample 3 Shift	0.0005	0.0003	0.0004
Data Shift	-0.0015	0.0013	0.0000
Shift Differences	Positive Charge	Negative Charge	Combined Average
Data & Sample 1 Shift Diff	0.0012	-0.0007	0.0002
Data & Sample 2 Shift Diff	0.0011	-0.0009	0.0001
Data & Sample 3 Shift Diff	0.0020	-0.0010	0.0004
Average Data & MC Shift Diff	0.0014	-0.0009	0.0002

Table 6: Example PID difference calculation.

E, M	16	20	21
1	0.0000 ± 0.0000	-0.0066 ± 0.0011	-0.0039 ± 0.0013
7	0.0002 ± 0.0002	-0.0062 ± 0.0011	-0.0037 ± 0.0014
8	0.0004 ± 0.0001	-0.0061 ± 0.0010	-0.0035 ± 0.0013

Table 7: Average monte carlo & detector data difference for each selector combination.

the average standard deviation of the rows and columns gives an approximation of the statistical uncertainty in the muon selector systematic error and the statistical uncertainty in the electron selector systematic error. This resulted in a systematic error of $\sigma_\mu = 0.00328 \pm 0.0005$ and $\sigma_e = 0.00021 + 0.00045$.

3.3 Agreement Between Monte Carlo and Data

While attempting to estimate the systematic uncertainty in the PID selectors, it was noted that when looking at the ratio histograms, there was a large disagreement between monte carlo and detector data. An example of this can be seen in Figure 3, where the same cuts as in Sections 3.2, that is no $\cos\theta$ cut was applied, and the PID selectors used were electron selector = 1 and muon selector = 16.
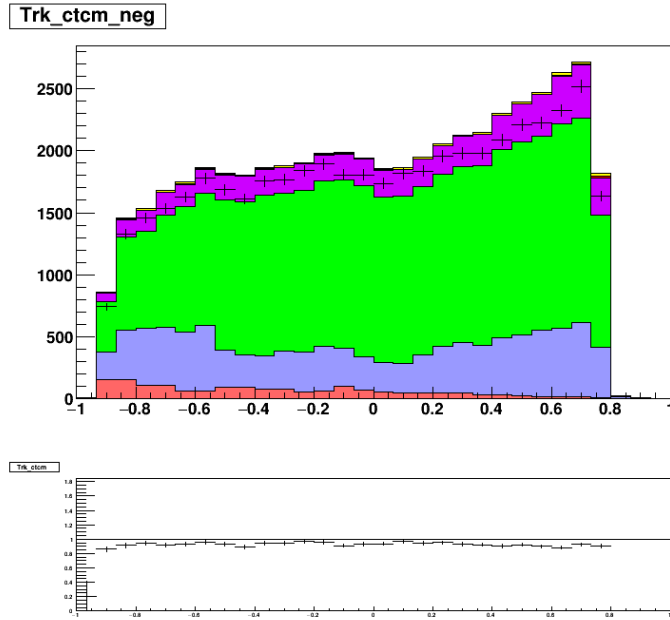
Figure 3: Monte carlo, detector data, and ratio histogram when $P_T > 1.2$ GeV. Note electron selector = 1 and muon selector = 16 were used.

This was also noted when $\frac{\chi^2}{N}$ was calculated using ratio histograms of different variables, with $\frac{\chi^2}{N} = 19.0875$ for the negatively charged signal track ctcm ratio histogram. Initially, this disagreement was thought to be due to two-photon events which were not reflected in the monte carlo data. These two-photon events could be cut out of the detector with an appropriate P_T cut. As such, using electron selector = 1 and muon selector = 16 and the same cuts as previously applied except for the P_T cut, $\frac{\chi^2}{N}$ was calculated for ratio histograms of different variables with varying minimum P_T (P_T^{min}) cuts to determine if adjusting the P_T^{min} would result in a reasonable agreement. Histograms were also plotted for varying P_T^{min} as seen in

13

Appendix B. As seen in Table 8, while changing the P_T^{min} to 1.4 GeV did improve the agreement between monte carlo and detector data when the other cuts and PID selectors were in place, there was still a large disagreement indicating that the two photon events were not the only reason for the disagreement.

P_T^{min} (GeV)	χ^2	N	$\frac{\chi^2}{N}$
1.6	484.663	30	16.1554
1.5	497.669	30	16.589
1.4	332.018	30	11.0673
1.3	507.254	30	16.9085
1.2	572.624	30	19.0875
1.1	549.446	30	18.3149
1.0	532.66	30	17.7553
0.9	500.734	30	16.6911
0.8	523.818	30	17.4606
0.7	375.093	30	12.5031
0.6	508.148	30	16.9383

Table 8: Agreement between monte carlo and detector data for ctcm of the negatively charged signal track using different P_T^{min}.

As changing the P_T^{min} did not improve the agreement, the disagreement was then thought to be due to an incorrect luminosity scaling. As the number of monte carlo events generated for each particle was significantly different from the expected amount of generated data, each of the monte carlo histograms in the monte carlo stack had a luminosity scaling applied to it. Thus an incorrect luminosity scaling could cause the monte carlo data to disagree with the detector data. As such, the luminosity scaling formula given in Equation 3 was written into the code and applied to the monte carlo histograms.

$$Scaling = \frac{1000000 * xsec * runlumi}{events},$$ (3)

In Equation 3, *xsec* is the cross section of the particle the monte carlo corresponds to, *events* is the total number of monte carlo events generated for that particle, and runlumi is the run luminosity of the detector. Run luminosity was changed to runlumi = 34.723 fb^{-1} to give the new luminosity scaling [3]. The cross section of

different particles and the total number of monte carlo events generated are shown in Table 9.

Particle	xsec (nb)	events
tau	0.919	117694000
bhabha	25.52	407500000
muon	1.147	76031000
uds	2.1	275849000
ccbar	1.3	88171000

Table 9: Cross section and total number of monte carlo *events* for each particle.

This luminosity scaling was applied to all the histograms in the monte carlo stacks for the different variables. When the same cuts that were previously applied, with the exceptions being P_T was now required to be greater than 1.4 GeV and $\cos\theta$ was required to be between -0.8 and 0.8 again, were applied to these monte carlo, the plots like the example seen in Figure 4 were created.
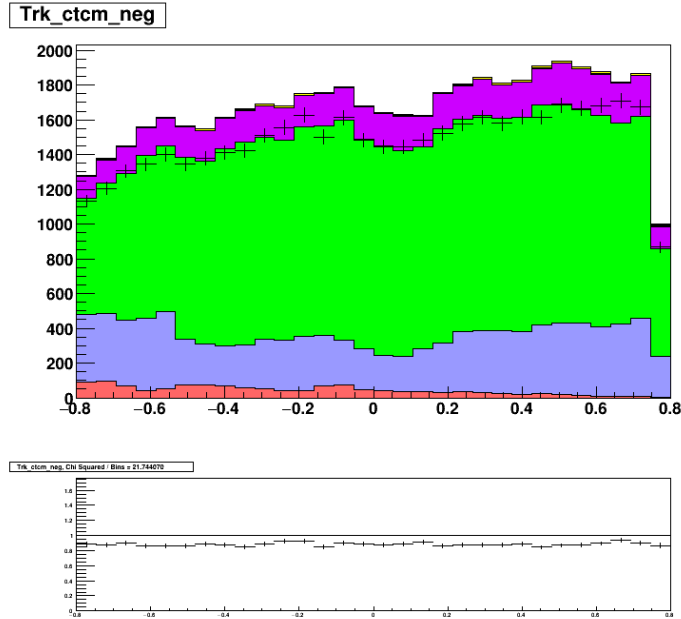
Figure 4: Histograms using corrected luminosity scaling. $\frac{\chi^2}{N} = 21.74$.

It was found for this plot that $\frac{\chi^2}{N} = 21.74$ was much greater than 1, indicating a

larger disagreement than seen with the previous luminosity scaling when P_T^{min} was 1.4 GeV (see Table 8). This can also be seen by looking at the ratio histogram seen in Figure 4. As the cross section of particles that were the largest components of the monte carlo data are well known, the number of monte carlo events for each particle are known exactly, and the run luminosity value was trusted, at the time there was no reason to believe that the luminosity scaling was incorrect. As such, changing the cuts to improve agreement was attempted first.

In order to determine which cuts provided the best agreement, all cuts were removed from monte carlo and detector data. New cuts were tested by looking at the histograms of different variables, determining regions on these histograms where there were large disagreements, and applying cuts to those regions. Cuts on regions where there were not many of the desired decays, τ to π decays for the signal track variables and τ to ρ decays for the tag track variables, and where there were many of the non-desired decays were also tested. If the cut gave a $\frac{\chi^2}{N}$ value closer to 1 and if that change also appeared to be due to the bins in the ratio histograms moving closer to 1, then those cuts were added. How the ratio histograms looked were taken into consideration because some tested cuts did give a $\frac{\chi^2}{N}$ value closer to 1, but only because they increased the error in the ratio histograms bins, not because the monte carlo and detector data had a better agreement.

After going through this process, the requirements that changed were that either π^0 mass now had to be greater than 0.11 GeV or π^0 likelihood had to be greater than 0, and the P_T had to be greater than 1.2 GeV. A new cut that was added was that the energy over momentum of the signal track pion had to be less than 0.9. Other than that, all previous requirements, including the requirement that $|\cos\theta|$ be less than 0.8 and that the PID selectors were electron selector = 1 and muon selector = 16, remained the same.

One thing of note is that there was difficulty determining, with the other new cuts and requirements, whether P_T greater than 1.2 GeV or P_T greater than 1.4 GeV provided better agreement. As agreement with both P_T^{min} was similar, polarization fits using the other new cuts and requirements were done for each P_T^{min}. Looking at goodness of fit scores for these fits, which can be seen in Table 10, it was determined that a better goodness of fit score occurred when the P_T^{min} was 1.2 GeV. As such, that P_T cut was chosen.

After applying these requirements, plots of different variables were created, an

16

P_T^{min} (GeV)	$(P_i^A - 0)^2$	$(\sigma_i^A)^2$	$(P_i^+ - P_i^-)^2$	Total Score
1.2	0.00001600	0.00034969	0.00108900	0.00145469
1.4	0.00007056	0.00043264	0.00366025	0.00416345

Table 10: Goodness of fit scores using new cuts for $P_T > 1.2$ and $P_T > 1.4$.

example of which can be seen in Figure 5. In Figure 5, it was found for the ratio histogram that $\frac{\chi^2}{N} = 19.38$. While the ratio histogram and $\frac{\chi^2}{N}$ value did show better agreement, $\frac{\chi^2}{N}$ was still much greater than 1 indicating there was still a large disagreement.
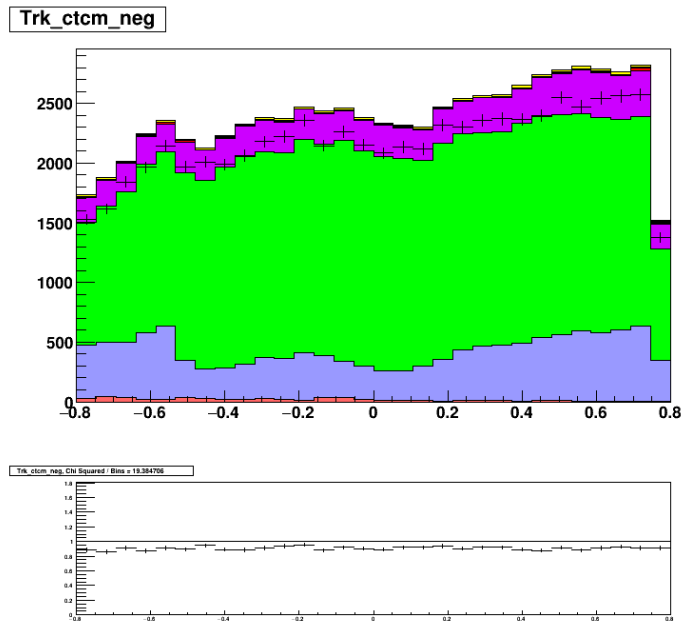
Figure 5: Histograms using new cuts. $\frac{\chi^2}{N} = 19.384706$.

As the disagreement could not be resolved by adjusting the cuts, the luminosity scaling was investigated to see if there existed a luminosity scaling that resulted in a $\frac{\chi^2}{N}$ closer to 1. As the cross sections of the particles that made significant contributions were well known and the number of monte carlo events per particle were known exactly, it was decided to adjust the run luminosity through trial and error until a run luminosity was found that gave a $\frac{\chi^2}{N}$ that was closer to 1. When

the run luminosity was changed to 31.12 fb^{-1}, the $\frac{\chi^2}{N}$ value closest to 1 was found and resulted in the example plot seen in Figure 6.
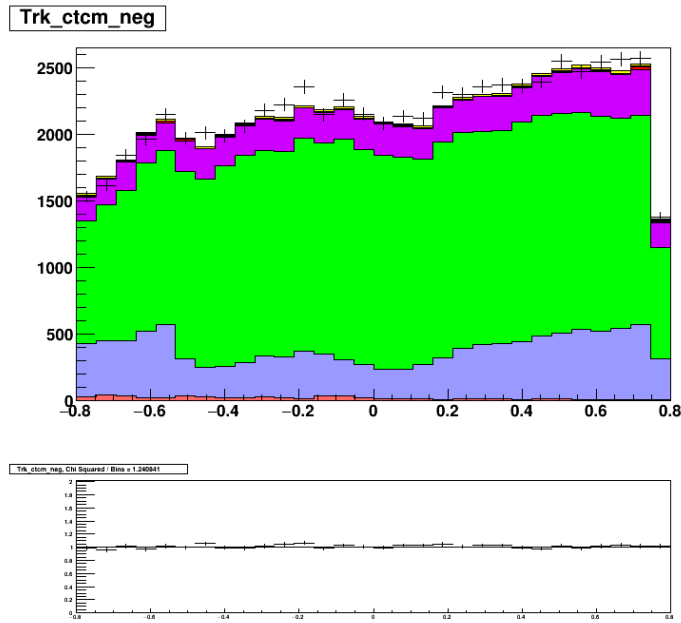
Figure 6: Histograms using new run luminosity. $\frac{\chi^2}{N}$ = 1.24.

Using the ratio histogram, it was found that $\frac{\chi^2}{N}$ = 1.24 and that the p-value = 0.1707, indicating the agreement between monte carlo and data had improved. This is also reflected in Figure 6 with the bins in the ratio histogram oscillating closely across 1. It should be noted that this does not indicate that the run luminosity was the issue. It only indicates that the agreement issue could be resolved by adjusting the run luminosity. At the time of writing this report, it is unknown what the true cause of the disagreement is. Further investigation will need to be done into this issue to determine whether the run luminosity or the luminosity scaling is the cause of the disagreement, or if there is another unknown cause for the disagreement.

3.4 Summary

Through an investigation of how PID selectors affect monte carlo data and polarization fits, it was found that electron selector = 1 and muon selector = 20 appeared to provide the best polarization fit. When the systematic error was estimated using the difference between PID selectors, the systematic errors due to the muon and electron selectors was found to be $\sigma_\mu = 0.00328 \pm 0.0005$ and $\sigma_e = 0.00021 + 0.00045$. When attempting to improve agreement, it was found that while adjusting the applied cuts did not improve agreement significantly, by adjusting the run luminosity from 34.723 fb^{-1} to 31.12 fb^{-1} while using the new cuts and luminosity scaling formula, the agreement could be increased to $\frac{\chi^2}{N} = 1.24$ with a p-value of 0.1707. It is unknown if the run luminosity is the true cause of this disagreement or if there is another unknown cause.

4 The Belle II Experiment

4.1 Introduction

The process for analyzing data in Belle II is similar to BaBar in the sense that events first needed to be reconstructed using monte carlo or detector data before such data could be used to create histograms or do polarization fits. Neither the Belle II analysis tools nor Belle II data used for reconstructing events had been used up to this point for this type of analysis. As such, the work done thus far with Belle II mainly focused on testing the Belle II analysis software and learning how to reconstruct particles and create histograms of variables such as centre of mass momentum and ctcm using the reconstructed data. As no proper analysis had been done yet by the tau group using the Belle II software, this section of the report will focus on a few issues found while testing the analysis software. Note that this testing was done using release-04-02-08 and release-05-00-00 of the Belle II analysis software.

4.2 Testing of Belle II Analysis Software

The first thing of note is an issue that was found while attempting to run the B2T_Basics_3_FirstAnalysis tutorial in the b2-starterkit. When attempting to run this tutorial, an error occurred when reconstructing events that caused the processing of events to fail. This error did not occur when the tutorial was run on another computer, indicating an issue isolated to the initial computer. After attempting to troubleshoot the issue, this issue was brought to the Belle II questions forum where a user, Sam Cunliffe, assisted in troubleshooting this issue. With his help, it was determined that the error was caused by a bonsai tree ASCII art outputted by TreeFitter during processing containing unsupported characters. Changing the locale to en_US.UTF-8 resolved the issue.

Another issue that was found was an issue that appeared when attempting to do a simple reconstruction of $\tau + \tau^- \to \pi^+ \bar{\nu}_\tau + \rho^- \nu_\tau$ events using the analysis software and a root file containing generated monte carlo events. When attempting to do this reconstruction, it was discovered that changing the decay string order during reconstruction changed the outputted root files containing those reconstructed particles.

Before showing some examples of those changes, a note needs to be made on decay string syntax. In the analysis package functions, the syntax of the decay strings is always "mother particle" arrow "daughter particle(s)". One thing to note though is that, as neutrinos are not detected by the detector, neutrinos are not included in the decay strings. As such, the decay string for $\tau^+ \to \pi^+ \nu_\tau$ is written without the neutrino as 'tau+:tauLabel $\to$ pi+:piLabel' within a function. Similarly, the decay string for $\tau^+ \to \pi^0 \pi^+ \nu_\tau$ is written as 'tau+:tauLabel $\to$ pi0:pi0Label pi+:piLabel'.

The goal was to reconstruct events using the $\tau + \tau^- \to \pi^+ \bar{\nu}_\tau + \rho^- \nu_\tau$ decays. As such, The decay strings used in the process of reconstructing events are the ones shown in Table 11.

When the order of 'tau+ $\to$ pi0 pi+' was changed to 'tau+ $\to$ pi+ pi0' when reconstructing the tag track, the value of the pi0 and pi+ variables in the outputted root file changed, and the gamma variables returned nan in the same root files, which can be seen in Figure 7

Decay	Belle II Decay String
$\pi^0 \to \gamma\gamma$	pi0:gg $\to$ gamma:good gamma:good
$\tau^+ \to \pi^0 \pi^+ \bar{\nu}_\tau$	tau+:tag $\to$ pi0:gg pi+:tag
$\tau^- \to \pi^- \nu_\tau$	tau-:signal $\to$ pi-:good
$\gamma \to \tau^+ \tau^-$	vpho:all $\to$ tau+:tag tau-:signal

Table 11: Decays and corresponding decay strings used when reconstructing events.


```
tau_0_pi0_gamma_0_M = 0                                    tau_0_pi0_gamma_0_M = nan
tau_0_pi0_gamma_0_ErrM = -nan                              tau_0_pi0_gamma_0_ErrM = nan
tau_0_pi0_gamma_0_SigM = -nan                              tau_0_pi0_gamma_0_SigM = nan
tau_0_pi0_gamma_0_InvM = 0                                 tau_0_pi0_gamma_0_InvM = nan
tau_0_pi0_gamma_0_px = 0.162233                            tau_0_pi0_gamma_0_px = nan
tau_0_pi0_gamma_0_py = -0.117215                           tau_0_pi0_gamma_0_py = nan
tau_0_pi0_gamma_0_pz = 0.200225                            tau_0_pi0_gamma_0_pz = nan
tau_0_pi0_gamma_0_pt = 0.200148                            tau_0_pi0_gamma_0_pt = nan
tau_0_pi0_gamma_0_p = 0.283106                             tau_0_pi0_gamma_0_p = nan
tau_0_pi0_gamma_0_E = 0.283106                             tau_0_pi0_gamma_0_E = nan
tau_0_pi0_gamma_0_isSignalAcceptMissingNeutrino = 1        tau_0_pi0_gamma_0_isSignalAcceptMissingNeutrino = nan
tau_0_pi0_gamma_1_M = 0                                    tau_0_pi0_gamma_1_M = nan
tau_0_pi0_gamma_1_ErrM = -nan                              tau_0_pi0_gamma_1_ErrM = nan
tau_0_pi0_gamma_1_SigM = -nan                              tau_0_pi0_gamma_1_SigM = nan
tau_0_pi0_gamma_1_InvM = 0                                 tau_0_pi0_gamma_1_InvM = nan
tau_0_pi0_gamma_1_px = 0.904641                            tau_0_pi0_gamma_1_px = nan
tau_0_pi0_gamma_1_py = -0.664631                           tau_0_pi0_gamma_1_py = nan
tau_0_pi0_gamma_1_pz = 1.63686                             tau_0_pi0_gamma_1_pz = nan
tau_0_pi0_gamma_1_pt = 1.12255                             tau_0_pi0_gamma_1_pt = nan
tau_0_pi0_gamma_1_p = 1.9848                               tau_0_pi0_gamma_1_p = nan
tau_0_pi0_gamma_1_E = 1.9848                               tau_0_pi0_gamma_1_E = nan
tau_0_pi0_gamma_1_isSignalAcceptMissingNeutrino = 1        tau_0_pi0_gamma_1_isSignalAcceptMissingNeutrino = nan
```

Figure 7: Differences in outputted root files when using decay strings 'tau+ $\to$ pi0 pi+' (left) and 'tau+ $\to$ pi+ pi0' (right).

When 'vpho:all $\to$ tau+:tag tau-:signal' was changed to 'vpho:all $\to$ tau-:signal tau+:tag' when reconstructing vpho, the number of candidates stored in the root file dropped to 0, as seen in Figure 8

```
*****************************************************************************
*Tree    :tau      :                                                        *
*Entries :     63545 : Total =            47521130 bytes  File  Size =    21374131 *
*        :          : Tree compression factor =   2.22                      *
*****************************************************************************
*****************************************************************************
*Tree    :tau      :                                                        *
*Entries :         0 : Total =              49041 bytes  File  Size =        3672 *
*        :          : Tree compression factor =   1.00                      *
*****************************************************************************
```

Figure 8: Differences in outputted root files when using decay strings 'vpho:all $\to$ tau+:signal tau-:tag' (top) and 'vpho:all $\to$ tau-:tag tau+:signal' (bottom).

It should be noted that the effects of changing the decay string were not investigated thoroughly, that is it was not tested with other decays, and the only effects found were the ones found during the process of learning how to reconstruct events with $\tau + \tau^- \rightarrow \pi^+ \bar{\nu}_\tau + \rho^- \nu_\tau$ decays.

Something else that was noticed during testing was that certain cuts needed to be applied during reconstruction to use some variables associated with the reconstructed particles. For instance, when the π^0 mass window was not applied during reconstruction, the analysis software was unable to match the reconstructed particles with their monte carlo pdg codes. This should be kept in mind if variables appear to be behaving unexpectedly.

The last thing that was accomplished before the work term had ended was the adjustment of the plotting macros to create histograms of variables from Belle II outputted root files. Once this was accomplished, it was noted that a lot more $\tau \rightarrow \rho$ and $\tau \rightarrow$ else decays were being reconstructed as $\tau \rightarrow \pi$ decays than expected, as seen in Figure 9.
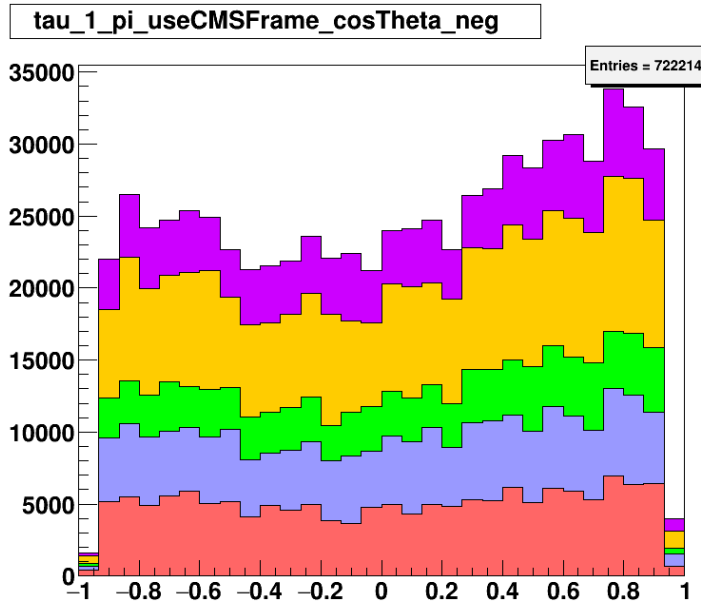
Figure 9: ctcm plot created using The Belle II monte carlo data without quality cuts. See Table 2 for colour scheme.

22

Initially this was thought to be due to a lack of quality cuts. At the time of writing, standard particle lists created for Belle II had not yet been approved for use during analysis. With no quality cuts applied then, the only other cuts applied were the requirements that there be only 2 tracks, that those tracks be in opposite hemispheres, and that on the signal track side there be no π^0 or γ. As such, to reduce the number of unwanted decays with the histograms, a few additional cuts were applied which include that the max distance of closest approach in the xy plane be 1.5 cm, max distance of closest approach in the z plane be 2.5 cm, that the π^0 mass window be from 0.115 GeV to 0.15 GeV, and that there be at most 2 photons in the tag track hemisphere. Despite these cuts, the same issues from the previous histograms still persisted, as seen in Figure 10.
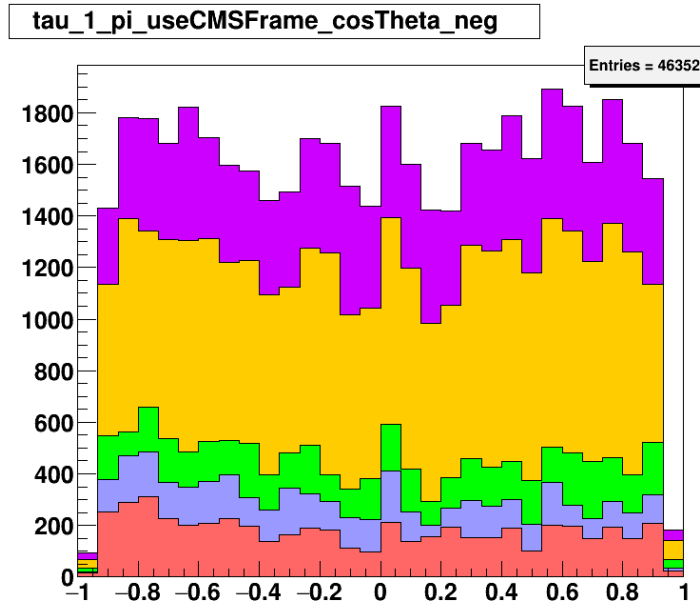
Figure 10: ctcm plot created using The Belle II monte carlo data without quality cuts.

It was thought that there was potentially a misunderstanding with which variables corresponded to which track, i.e. whether a variable belonged to the signal track or the tag track. To determine which variables belong to which track and particle, decay hashes were used to match reconstructed events with the full monte carlo decay string. While this method did determine that there was a misinterpretation with which variables corresponded to which particle, it also determined that

23

those variables were correctly associated with the proper track initially, meaning that was not the cause of the issue. Further investigation will need to be done to determine the root cause of the large amount of unexpected decays.

4.3 Summary

Testing was done with the Belle II analysis software to learn how to reconstruct events and use the reconstructed data for further analysis. While testing, it was determined that, if TreeFitter was used during reconstruction, an error could occur due to the TreeFitter bonsai tree ASCII art outputted during processing. This error can be avoided by using the en_US.UTF-8 locale. It was also determined that changing the order of the decay strings in the reconstruction code could change the values of the variables and the number of entries in the outputted root file containing the reconstructed data. Something else learned was that certain cuts needed to be applied during reconstruction to use some variables associated with the reconstructed particles. Finally, it was discovered that the amount of $\tau \rightarrow \rho \nu_\tau$ and $\tau \rightarrow$ else decays that made it through the Belle II reconstruction was far greater than expected. The addition of quality cuts did not reduce the number of unwanted decays, and it was determined that this issue was not due to a misassociation between the variables and the two tracks. At the time of writing this report, it is unknown where this large amount of unwanted decays comes from.

Appendices

A Other Histograms Used When Investigating PID Selectors

Figure 11 shows the other ctcm plots created when narrowing down the list of potential PID selectors.
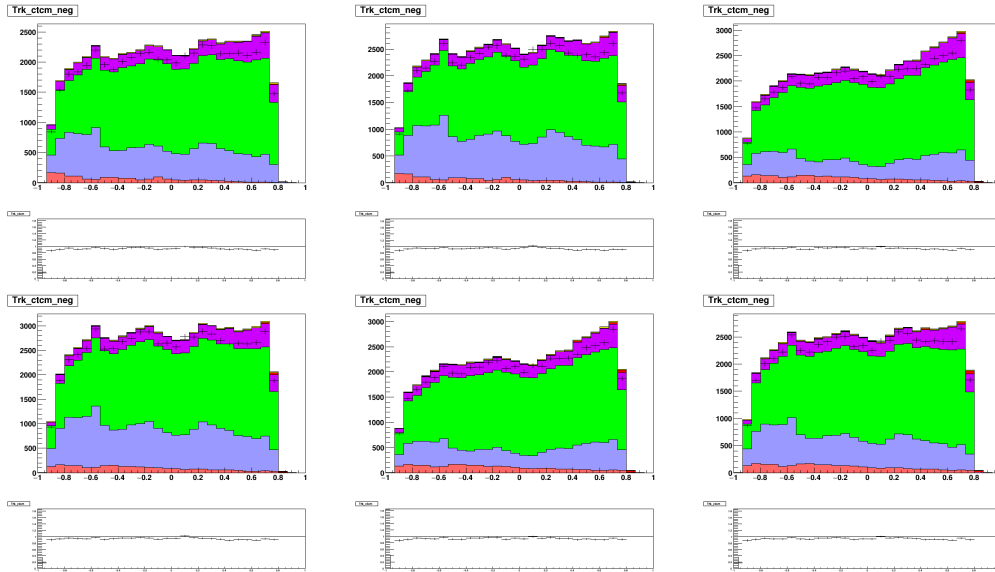
Figure 11: Other histograms left out of Figure 2. PID selectors used for each histogram were electron selector = 1, muon selector = 20 (top left), electron selector = 1, muon selector = 21 (top right), electron selector = 7, muon selector = 16 (middle left), electron selector = 7, muon selector = 21 (middle right), electron selector = 8, muon selector = 16 (bottom left), electron selector = 8, muon selector = 20 (bottom left).

B Histograms Used When Investigating P_T Cut

Figure 12 show the ctcm plots created while investigating how P_T affected agreement.
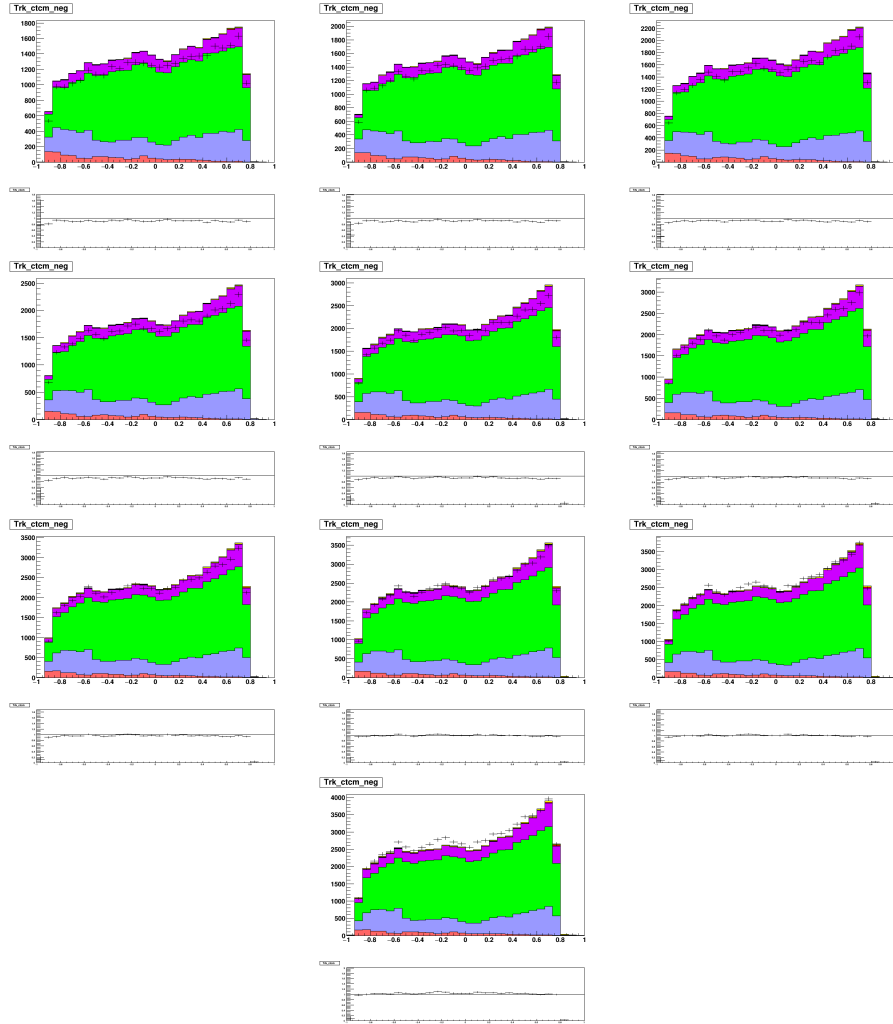
Figure 12: Histograms created when varying P_T^{min}. P_T^{min} used for each histogram was $P_T > 1.6$ (top left), $P_T > 1.5$ (top middle), $P_T > 1.4$ (top right), $P_T > 1.3$ (middle left), $P_T > 1.1$ (middle middle), $P_T > 1.0$ (middle right), $P_T > 0.9$ (bottom left), $P_T > 0.8$ (bottom middle), $P_T > 0.7$ (bottom right), $P_T > 0.6$ (last plot),

References

[1] J. Michael Roney. Electroweak physics with polarized electron beams in a superkekb upgrade. *Proceedings of Science*, pages 1–4, 2019.

[2] Roger Barlow and Christine Beeston. Fitting using finite monte carlo samples. *Computer Physics Communications*, 77:219–228, 1993.

[3] J. P. Lees, V. Poireau, V. Tisserand, N. Arnaud, M. Davier, D. Derkach, G. Grosdidier, F. Le Diberder, A. M. Lutz, B. Malaescu, P. Roudeau, M. H. Schune, A. Stocchi, G. Wormser, D. Bernard, M. Verderi, S. Emery, G. Hamel De Monchenault, G. Vasseur, Ch Yèche, S. Akar, E. Ben-Haim, M. Bomben, G. R. Bonneaud, H. Briand, G. Calderini, J. Chauvau, O. Hamon, Ph Leruste, G. Marchiori, J. Ocariz, and S. Sitt. Time-integrated luminosity recorded by the babar detector at the pep-ii e + e - collider. *Nuclear instruments methods in physics research. Section A, Accelerators, spectrometers, detectors and associated equipment*, 726:203–213, 2013.